COO-1248-35
Conf-730601--2

FLUID MECHANICS OF THE LAMINAR FLOW AEROSOL IMPACTOR

by Virgil A. Marple, Benjamin Y. H. Liu and Kenneth T. Whitby

Particle Technology Laboratory
Department of Mechanical Engineering
University of Minnesota
Minneapolis, Minnesota 55455

March 1973

Particle Technology Laboratory Publication No. 198

DISCLAIMER

ABSTRACT

A study has been made of the fluid mechanics of laminar flow aerosol impactors of both the rectangular and round geometry. Streamlines in a rectangular impactor were obtained theoretically by solving the Navier-Stokes equations on a computer. The results were found to be in good agreement with experimentally generated streamlines in a water model using an electrolytic flow visualization technique. Further theoretical studies of the impactor using the computer solution technique showed that the flow field in the impaction region above the impaction plate is influenced only to a very limited extent by the impactor throat length while the effect due to variations in the jet-to-plate distance and the jet Reynolds number is somewhat larger. The boundary layer thickness along the impaction plate was found to be nearly constant, but the thickness was dependent on the jet Reynolds number and affected to a very slight extent by the jet-to-plate distance.

FLUID MECHANICS OF THE LAMINAR FLOW AEROSOL IMPACTOR

by Virgil A. Marple, Benjamin Y. H. Liu and Kenneth T. Whitby

Introduction

The aerosol impactor, an inertial separation device for collecting air borne particles, has been widely used for sampling air borne particles for gravimetric, chemical, neutron-activation, and similar analyses to determine the mass concentration, particle size distribution, and chemical composition of the air borne particulates. The device has been extensively used in air pollution and industrial hygiene studies, and for assessing the characteristics and health hazards of air borne particulate matter in general. The instrument is relatively inexpensive, simple to operate, and has easily understood performance characteristics. However, its application is sometimes limited by the possibility of particle bounce and reentrainment, and, in the case of cascade impactors which are used for particle size distribution measurements, by the interstage particle loss which is not always known.

Since the first description of the cascade impactor by May (1945), numerous impactors have been designed and constructed for different applications. A summary of these studies is given in Tables 1 and 2 for both the rectangular and the round impactors. The pertinent operating conditions and other important data are also included in these tables.

In contrast to the many experimental studies that have been made on the impactor, there have only been a limited number of theoretical studies. One of the first such studies appears to be that of Baurmash et. al. (1949) as reported by Wilcox (1953). The simple theory of Baurmash assumes that the streamlines over the impaction plate are in the form of circular arcs. The resulting formula for the impaction efficiency is therefore very approximate.

Ranz and Wong (1952a) used a more realistic flow field corresponding to that of a frictionless stagnation flow in the vicinity of the stagnation point, and their theory was later improved and refined by Mercer and Chow (1958) and Mercer and Stafford (1959). A rigorous theoretical analysis based on the method of conformal mapping and the solution of the Euler's equation for the flow of a frictionless fluid through a rectangular impactor was given by Davis and Aylward (1951). However, due to viscous boundary layer effects of real fluids, a realistic analysis of the impactor must take into account frictional effects of the fluid for which a solution of the Navier-Stokes equations is needed. The purpose of this paper is to describe some theoretical studies based on the numerical solution of the Navier-Stokes equations on a digital computer. The theoretical flow fields have also been compared with experimental flow fields obtained by means of a water model. Results of these comparisons will also be presented. A summary of the approximate flow fields used by previous investigators is given in Table 3.

Impactor Flow Fields

An examination of the operating conditions of real impactors in Tables 1 and 2 shows that the operating Reynolds number covers a range between 80 and 22,000, with most impactors having a Reynolds number below 7000. In the case of a convergent flow in an impactor, the flow is probably laminar even for relatively high Reynolds numbers although the possibility of turbulence cannot be ruled out. Undoubtedly an impactor theory based upon turbulent flow would be more complicated than one based on laminar flow. We will assume in this analysis that the flow is laminar even for the higher Reynolds numbers.

Theoretical Flow Fields

Assuming laminar flow exists in the impactor, the Navier-Stokes equations can be applied. Although analytical solutions to the Navier-Stokes equations are often difficult, if not impossible, to obtain, numerical solutions can be obtained using finite difference methods with the aid of a digital computer. The method used in this analysis closely follows the general solution procedure described by Gossman, et. al. (1969).

The derivation of the finite difference equation and the corresponding computer program is given in detail by Marple (1970). The method of analysis applies equally well to rectangular and round impactors. The flow field is assumed to be in the x-y plane of a rectangular coordinate system or the r-z plane of a cylindrical coordinate system for the rectangular and round impactors respectively.

The general method of solution is first to express the Navier-Stokes equations, in the desired coordinate system, in terms of the vorticity and the stream function. The resulting differential equations are then expressed in a finite difference form and solved by the method of relaxation over a grid of node points covering the field of interest.

Experimental Flow Field

In order to insure that the flow field obtained from the theoretical analysis was correct, the theoretical streamlines were compared with streamlines observed in a water model of the same identical geometry and operated at the same Reynolds number. The water model used a flow visualization technique based on a method reported by Baker (1966) in which an electrolyte pH indicator is used. Dark, visible streamlines were generated by means of metal wires held at some negative potential which changed the local pH, and

hence the color of the solution. A modelling facility was set up which provided a continuous flow of the solution through the impactor model. The clear Plexiglas model was completely immersed in the liquid solution in a glass tank, thus providing a liquid-liquid interface along the free streamlines emerging from the impactor exit. Photography was used to record the streamlines for subsequent analysis. A detailed description of this modelling facility has been given by Marple (1970).

The contour shape of the model for the two dimensional rectangular impactor is shown in Figure 1. This model was designed so that both the impaction plate and the two horizontal plates above it could be adjusted. A perforated plate was placed transversely across the entrance to provide a flat velocity profile, thus providing a known flow condition at the entrance. The streamlines were traced by locating nine equally spaced electrodes across the impactor's entrance. These electrodes were insulated wires stretched parallel to the long direction of the rectangular jet with 1/8 inch of the insulation scraped off at the center of each wire to effectively provide a point electrode for generating the dark traces.

The throat of the impactor model is 2 centimeters wide by 20.3 centimeters long. Since the streamlines were generated at the center of the long dimension of the jet to avoid end effects, the data taken can be considered as those for a two-dimensional jet. The Reynolds number was based on the hydraulic diameter which is twice the jet width ($Re = \frac{\rho Vo\ 2W}{\mu}$) for a two-dimensional jet of infinite length-to-width ratio.

Comparison of Theoretical and Experimental Flow Fields

A comparison of the theoretical and experimental flow fields was made by solving the finite difference flow field equations for the configuration of the water model (Figure 1), assuming a flat velocity profile at the impactor

entrance. In order to insure that the position of the resulting theoretical streamlines was not influenced by the size of the grid spacing over which the finite difference equations were solved, several spacings were tried. Although they all gave basically the same results, the grid spacing which gave good accuracy and yet did not take excessively long computer time is the 18 by 36 line grid indicated in Figure 2. To insure that its flow field would not change drastically if a smaller grid spacing was used, a finer grid with half the regular grid spacing was also used for one case. A comparison was then made of the corresponding theoretical results. This comparison, shown in Figure 2, reveals that using the smaller grid has only a slight effect on the position of the streamlines. Thus the larger grid spacing was felt to be a good compromise between accuracy and computer time.

In Figure 3, the theoretical and experimental streamlines for a rectangular impactor are compared for $S/W = 1$, where S is the jet-to-plate distance, and W is the jet width, and Reynolds numbers of 700 and 2300, which represent the two extreme cases studied experimentally. The experimental streamlines were taken from photographs similar to that shown in Figure 1. Their positions were measured from the center streamline and corresponding streamlines on either side of center were averaged. This technique corrected for the slight asymmetry in the experimental flow fields. The theoretical streamlines were started on the second grid line which was approximately where the wires were located in the model.

The comparison in Figure 3 shows that there is satisfactory agreement between the experimental and theoretical streamlines. The agreement in the throat and impaction regions is within the accuracy with which the position of experimental streamlines could be determined. However, some discrepancies can be noted in the entrance region of the jet, and they appear to be due to errors in the theoretical calculations resulting from the finite grid

spacing used. Figure 2 shows that the theoretical streamlines obtained when the grid spacing is halved are closer to the experimental results. Thus if the grid spacing were made still smaller, better agreement could be expected.

In order to further verify the validity of the calculation procedure and computer program, the flow field in the entrance region of a parallel plate channel was analyzed using the grid pattern shown in Figure 4. An analytical solution for this case has been obtained by Sparrow, et. al. (1964) and can be used for comparison with the present finite difference numerical solution. A uniform velocity profile was assumed at the entrance in both cases and the Reynolds number based on twice the jet width was 1000.

The velocity profiles are compared in Figure 4 at positions, y, corresponding to 0.5, 1.5, and 3.0 W from the entrance, where W is the channel width. The velocity profiles given by these two different methods are seen to agree well, the greatest discrepancy being at y = 0.5 W. However, the center-line velocity at this position disagree by only about 1%.

Theoretical Flow Fields for Round and Rectangular Impactors

The above comparisons show that the numerical solution procedure can be used with confidence for determining the flow fields of rectangular impactors. Therefore this approach was used to study the rectangular impactor by systematically varying the jet-to-plate distance, jet Reynolds number, and jet throat length. By making the appropriate changes in the governing equations of the computer program, the same approach can be used to study the round impactor.

The contour shape and the corresponding grid lines used for the rectangular and the round impactors are shown in Figures 5 and 9. Both cases have convergent entrances and straight throat sections. Having a longer entrance

section was found to be unnecessary for the theoretical calculations since the resulting flow fields in the throat and impaction regions are essentially the same as for the case shown.

The grid lines shown along the contour in Figure 5 are for S/W = 0.5 and for T/W = 2, where T is the throat length of the impactor. For S/W less than 0.5, the same number of grid lines between the jet axis and the impaction plate were used; only their spacing changed. However, for jet-to-plate distances larger than 0.5, more grid lines were added, thus keeping the grid spacing of the 10 grid lines above the impaction plate the same as in Figure 5. Likewise the throat length was varied by changing the number of grid lines in this section while keeping the grid spacing constant.

To determine the influence of the jet-to-plate distance on the flow field of the rectangular impactor, the Reynolds number was kept at 3000 and the T/W ratio was fixed at one. S/W ratios of 0.25, 0.5, 1, 2, and 5, were used.

The streamlines and some velocity profiles for four jet-to-plate distances are shown in Figures 5 and 6. The streamlines through the entire impactor are shown only for S/W = 1 and are designated by both the stream function and $q = 1 - \frac{\psi}{0.5}$, where q is the fraction of the total volumetric flow between the streamline of interest and the stagnation streamlines along the impactor axis.

It can be seen in Figure 6 that the free streamline emanating from the impactor wall has reattached to the upper boundary of the horizontal section for S/W = 0.25 and is nearly attached for S/W = 0.5. Also, these figures show that the flow field in the impaction region, i.e., the region above the impaction plate where the streamlines make substantial changes in direction, is nearly the same for S/W = 1 and 5.

The details of the flow along the impaction plate is made clearer by the velocity profiles along the impaction plate, as shown in Figure 7. This again

shows that there is little change in the flow field near the impaction plate for $S/W \geq 1$. It is interesting to note that the boundary layer thickness along the impaction plate is nearly equal for the three jet-to-plate distances shown.

A theoretical study of the flow fields in rectangular impactors was also made by Davies and Aylward (1951) using the method of conformal mapping. In their theory the velocity ratio

$$\alpha = \frac{U_o}{V_o} = \frac{\text{mean fluid velocity at impactor exit}}{\text{mean fluid velocity at impactor throat}} \qquad (1)$$

is introduced, and the value of this quantity is determined from the asymptotic position of the free streamline from the impaction plate as follows:

$$\alpha = \frac{W/2}{\text{Distance of free streamline from impaction plate}} \qquad (2)$$

On the basis of the present work, the free streamline emanating from the impactor throat wall is seen to reattach to the upper boundary of the horizontal section for small jet-to-plate distances. This can be seen in Figure 6 for $S/W = 0.25$. The same phenomenon was also observed in the modelling studies. Thus, for sufficiently small jet-to-plate distances, α is given by

$$\alpha = \frac{W/2}{S} = \frac{1}{2(S/W)} \qquad (3)$$

On the other hand, a closer examination of Figures 5 and 6 shows that for $S/W \geq 1$ the value of α as given by Equation 2 is approximately equal to one. The exact value of α for a given S/W ratio will, of course, depend on the Reynolds number and to a lesser extent on the exact length of the horizontal section which has been set to 1.5 W for the present study. The value of α for the particular impactor under consideration is shown plotted as a function of S/W in Figure 8 together with the values predicted by the potential flow theory of Davies and Aylward (1951) and experimental data of Mercer and Chow (1968), the latter being obtained from pressure drop measurements. Note the good agreement

between the present theoretical work and the experimental data.

For the case of the round impactor, the Reynolds number was kept at 3000 and the T/W ratio was fixed at 2, where W now denotes the throat diameter. S/W ratios of 0.125, 0.25, 0.375, 0.5, 2, and 5 were used. Figures 9 and 10 present the streamlines and velocity profiles for four S/W ratios. For the round impactor, $q = 1 - \frac{\psi}{0.125}$, and is numerically equal to the fraction of volumetric flow within that streamline.

It is of interest to note in Figure 10 that, unlike the rectangular impactor, the free streamline does not reattach in the round impactor for S/W ratios as small as 0.125 and Re = 3000. However, as will be seen later, reattachment of the free streamline does occur when the Reynolds number is sufficiently small.

Similar to the case for the rectangular impactor, there is a critical point beyond which further increases in the S/W ratio appear to have little effect on the flow field in the impaction region. For the round impactor this occurs at about S/W = 0.5. This feature can also be seen in Figure 11, which shows the velocity profiles along the impaction plate for S/W = 0.25, 0.5, and 5. Figure 11 not only shows that increasing S/W beyond 0.5 does not greatly change the velocity profile along the plate, but that the boundary layer thickness is unaffected by the actual jet-to-plate distance.

To study the effect of the jet Reynolds number on the flow field, the S/W ratio for the rectangular and the round impactor was kept at 1 and 0.5 respectively. The T/W ratio was held at 1 for both impactors while the Reynolds numbers were set at 10, 100, 500, 3000, and 25,000. The streamlines for four Reynolds numbers are shown in Figures 5 and 12 for the rectangular impactor. Only the flow field for Re = 3000 is shown for the round impactor in Figure 9. For other values of Re, excluding Re = 10, the streamlines in the

round impactor were similar to those shown in Figure 9, and the distance between the free streamline and the impaction plate was found to increase with decreasing Reynolds numbers. When Re = 10 the flow fills the region above the impaction plate similar to that for the rectangular impactor at Re = 10.

This study shows that the flow is changing continuously over this range of Reynolds numbers. At Re = 10 the flow fills the entire channel above the impaction plate. At Re = 100 the free streamline reattached to the upper plate for the rectangular impactor, but did not for the round impactor. For the three larger Reynolds numbers, the free streamline did not reattach. These figures also show that the boundary layer along the impaction plate becomes thinner as the Reynolds number is increased.

More can be seen about this boundary layer from the velocity profiles above the impaction plate in Figure 13 where the velocity profiles and free streamlines are shown at Re = 10, 3000, and 25,000 for both the rectangular and round impactors. In both cases there is a large change in the velocity profile from Re = 10 to Re = 3000 and relatively small changes in the profile from Re = 3000 to Re = 25,000. However, it is of interest to note that the boundary layer thickness remains essentially constant along the impaction plate and is smaller for Re = 25,000 than for Re = 3000.

In order to further define the flow field, the velocity profiles at the throat exit are shown in Figure 14 for both impactors. At low Reynolds numbers (Re = 10 and 100), the velocity reaches a maximum at the centerline and decreases steadily toward the wall. At larger Reynolds numbers ($Re \geq 3000$ for the rectangular impactor and $Re \geq 500$ for the round impactor) the velocity profile is relatively flat over the center half of the jet. Also shown for the round impactor is the theoretical velocity profile for the case of the potential flow of an inviscid fluid (Luna, 1965) for a jet-to-

plate distance of 0.5. For this case the maximum velocity occurs at the wall because of the potential flow assumption.

The effect of the throat length on the flow field was found to be negligible for the round impactor when the T/W ratio was changed from 0 to 0.25, 1, and 2. The Reynolds number was constant at 3000 and the jet-to-plate distance was 0.5. For all four cases the flow field above the impaction plate was nearly the same as that shown in Figure 9.

For the case of the rectangular impactor, the T/W ratio was set at 1 and 10 with Re = 3000 and S/W = 1. Results similar to those for the round impactor were obtained, indicating a negligible effect on the flow field above the impaction plate.

ACKNOWLEDGEMENT

This research was supported in part under an AEC contract AT(11-1)-1248 and in part by an NSF traineeship. We wish to thank the Numerical Analysis Center, University of Minnesota, for the use of the CDC 6600 digital computing facilities. This paper carries the publication number COO-1248-32 under the AEC contract.

NOMENCLATURE

q = fraction of total flow between the streamline of interest and the stagnation streamline along the impactor axis

Re = Reynolds number $= \frac{\rho V_o 2W}{\mu}$ for rectangular impactor

$= \frac{\rho V_o W}{\mu}$ for round impactor

r' = radial distance from jet axis, cm

r = r'/W

S = jet-to-plate distance, cm

T = throat length, cm

U_o = mean fluid velocity at impactor exit, cm/sec

V_o = mean fluid velocity at throat, cm/sec

V_x = x-component of fluid velocity, cm/sec

V_y = y-component of fluid velocity, cm/sec

V_r = r-component of fluid velocity, cm/sec

V_z = z-component of fluid velocity, cm/sec

V_x = V_x'/V_o

V_y = V_y'/V_o

V_r = V_r'/V_o

V_z = V_z'/V_o

W = jet width for rectangular impactor, cm
jet diameter for round impactor, cm

x' = transverse distance from jet axis, cm

x = x'/W

y' = longitudinal distance from entrance, cm

y = y'/W

z' = axial distance from entrance, cm

z = z'/W

$\alpha = \frac{U_o}{V_o}$

μ = fluid viscosity, poise

ξ' = normal distance from impaction plate, cm

$\xi = \frac{\xi'}{W}$

ρ = fluid density, gm/cm^3

ψ' = stream function, cm^2/sec for rectangular impactor
cm^3/sec for round impactor

ψ = ψ'/V_oW for rectangular impactor
ψ'/V_oW^2 for round impactor

Table 1 Experimental Studies of Rectangular Impactors

Reference	S/W	$Re = \frac{\rho D_h V_o}{\mu}$***	Pressure (atmospheres)	Type*	Special studies**	Aerosol
MAY (1945)	1/2-1	1400-2700	1	C(4)	a-b	Windborne
LIPPMAN (1959)	1/2-1	1400-2700	1	C(4)	a	Uranium oxides
WELLS (1967)	.46-.69	1400-2700	1	C(4)		Plutonium & Uranium oxides; Polystyrene spheres
DAVIES et al (1951)	1/2-1	1400-2700	1	C(5)	a-b	Coal dust
SONKIN (1946)		3000-5000	1	C(4)		Glycerol-water-methylene blue solution
LASKIN (1949)			1	C(4)		Uranium compounds
WILCOX (1953)		1850-6500	1	C(5)		
RANZ & WONG (1952a)	1-3	250-16,500	1	S		Glycerol
RANZ & WONG (1952b)	1-3	250-16,500	1	C(4)		Glycerol, Ammonium chloride & Sulfuric acid
STERN et al (1962)	.3-1	50-3500	.03-.25	S		Polystyrene spheres
LUNDGREN (1967)	1	600-6000	1	C(4)	a-b	Polystyrene spheres Uranine dye & Glass beads
MERCER & CHOW (1968)	3/8-5	1200-7000	1	S		Polyvinyltoluene spheres

*S - single stage impactor
C(n) - cascade impactor (number of stages)

**a - wall loss studies
b - particle bounce studies

***$D_h = 2W$

Table 2 Experimental Studies of Round Impactors

Reference	S/W	$Re = \frac{\rho D_h V_o}{\mu}$***	Pressure (atmospheres)	Type*	Special studies**	Aerosol
RANZ & WONG (1952a)	1-3	650-22,000	1	s		Glycerol
BRINK (1958)	3	1400-6900	1	C(5)		Sulfuric acid
PILCHER et. al. (1955)	3/8	1200-12,000	1	C(6)		Dibutyl phthalate & Polystyrene spheres
MITCHELL & PILCHER (1959)	3/8	1200-12,000	1	C(6)	a	Dibutyl phthalate & Polystyrene spheres
STERN et. al. (1962)	1/3-3		.03-.25	s		Polystyrene spheres
MCFARLAND & ZELLER (1963)	.34-1	18-650	.0013-.02	S-M	b	Methylene blue & Uranine dye
ZELLER (1965)	.34-1	18-650	.0013-.02	C(2)-M	b	
MAY (1966)	.375	5000-7500	1	C(3)		Dye particles
ANDERSEN (1958)	2-10	80-380	1	C(6)-M	a-b	Carnauba wax & Airborne Microorganisms
ANDERSEN (1966)	2-10	80-380	1	C(6)-M		Carnauba wax
FLESCH et. al. (1967)	2-10	80-380	1	C(6)-M		Methylene blue dye & Polystyrene spheres
PARKER & BUCHHOLZ (1968)	2-10 35-4		.05-1	C(6)-M C(6)-M	a-b	Sodium chloride, PbI $CsNO_3$, Uranine & Methylene blue plus Uranine
MAY (1964)	2-10	100-380	1	C(7)-M		Bacterial particles
MERCER & STAFFORD (1969)	3/8-10	600-7000	1	s	b	Polystyrene spheres
MCFARLAND & HUSAR (1967)	1-1.5	1500-1900	1	C(4)-M	b	Dye particles
MERCER et. al. (1970)	1-2	90-1300	1	C(7)	a	Cesium chloride

*S - single stage impactor
C(n) - cascade impactor (number of stages)
M - multiple jet

**a - wall loss studies
b - particle bounce studies

***D_h = W

Table 3 Theoretical Flow Fields

Reference	Flow Field
DAVIES & AYLWARD (1951)	Rectangular Impactor Ideal Fluid (Potential Flow)
RANZ & WONG (1952a)*	Rectangular Impactor $V_x = 2x$, $V_y = -2y$ for $-1/2<x<1/2$, $-1/2<y<0$ $V_y = 0$ for $-1/2>x>1/2$, $-1<y<0$ Round Impactor $V_r = 2r$, $V_z = -4z$ for $-1/2<r<1/2$, $-1/4<z<0$ $V_z = 0$ for $-1/2>r>1/2$, $-1/4<z<0$
MERCER & CHOW (1968)*	Rectangular Impactor $V_x = x/\beta$, $V_y = -y/\beta$ for $-(1+\Delta x)<x<(1+\Delta x)$, $-\beta<y<0$ $V_y = 0$ for $-(1+\Delta x)>x>(1+\Delta x)$, $-\beta<y<0$
MERCER & STAFFORD (1969)*	Round Impactor $V_z = -z/\beta$, $V_r = r/2\beta$ for $-(1+\Delta r)<r<(1+\Delta r)$, $-\beta<z<0$ $V_z = 0$ for $-(1+\Delta r)>r>(1+\Delta r)$, $-\beta<z<0$
WILCOX (1953)	Assume streamlines make a 90° turn

*

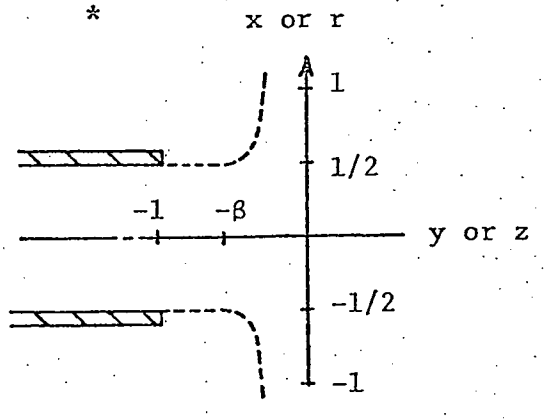

BIBLIOGRAPHY

Andersen, A. A. (1958) "New sampler for the collection, sizing, and enumeration of viable airborne particles," J. Bact., 76:471.

Andersen, A. A. (1966) "A sampler for respiratory health hazard assessment," Am. Ind. Hyg. Assoc. J., 27:160.

Baker, D. J. (1966) "A technique for the precise measurement of small fluid velocities," J. Fl. Mech., 26:573.

Brink, Jr., J. A., (1958) "Cascade impactor for adiabatic measurements," I & E Chem., 50:645.

Davies, C. N. and M. Aylward (1951) "The trajectories of heavy, solid particles in a two-dimensional jet of ideal fluid impinging normally upon a plate," Proc. Phys. Soc., (London) B, 64:889.

Davies, C. N., M. Aylward and D. Leacey (1951) "Impingement of dust from air jets," A.M.A. Arch. Ind. Hyg. Occup. Med., 4:354.

Flesch, J. P., C. H. Norris and A. E. Nugent, Jr. (1967) "Calibrating particulate air samplers with monodisperse aerosols: application to the Andersen cascade impactor," Am. Ind. Hyg. Assoc. J., 28:507.

Gousman, A. D., W. M. Pun, A. K. Runchal, D. B. Spalding and M. Wolfshtein (1969) Heat and Mass Transfer in Recirculating Flows, Academic Press, New York.

Laskin, S. (1949) in C. Voegtlin and H. C. Hodge, eds., Pharmacology and Toxicology of Uranium Compounds, 1:463-505, McGraw-Hill, New York.

Lippmann, M. (1959) "Review of cascade impactors for particle size analysis and a new calibration for the Casella cascade impactor" Am. Ind. Hyg. Assoc. J., 20:406.

Luna, R. E. (1965) "A study of impinging axisymmetric jets and their application to size classification of small particles" Ph.D. Thesis Department of Aerospace & Mechanical Sciences, Princeton University, Report No. 744.

Lundgren, D. A. (1967) "An aerosol sampler for determination of particle concentration of size and time," J. Air Poll. Cont. Assoc., 17:225.

Marple, V. A. (1970) "A fundamental study of inertial impactors," Ph.D. Thesis Mechanical Engineering Department, University of Minnesota, Particle Technology Laboratory Publication No. 144.

May, K. R. (1945) "The cascade impactor: an instrument for sampling coarse aerosols," J. Sci. Instr., 22:187.

May, K. R. (1964), "Calibration of a modified Andersen bacterial aerosol sampler," Appl. Microbiology, 12:37.

May, K. T. (1966) "Multistage liquid impinger," Bact. Revs., 30:559.

McFarland, A. R., and R. B. Husar (1967) "Development of a multistage inertial impactor," University of Minnesota Particle Technology Laboratory Publication No. 120.

McFarland, A. R., and H. W. Zeller (1963) "Study of a large-volume impactor for high-altitude aerosol collection, General Mills, Inc. Electronics Division, Report No. 2391, Contract AT(11-1)-401.

Mercer, T. T., and H. Y. Chow (1968) "Impaction from rectangular jets," J. Coll. and Interface Sci., 27:75.

Mercer, T. T., and R. G. Stafford (1969) "Impaction from round jets," Ann Occup. Hyg., 12:41.

Mercer, T. T., M. I. Tillery, and G. J. Newton (1970) "A multistage, low flow rate cascade impactor," Aerosol Science, 1:9.

Mitchell, R. I. and J. M. Pilcher (1959) "Improved cascade impactor for measuring aerosol particle sizes in air pollutants, commerical aerosols and cigarette smoke," I & E Chem., 51:1039.

Parker, G. W., and H. Buchholz (1968) "Size classification of submicron particles by a low-pressure cascade impactor" Oak Ridge National Laboratory Report ORNL-4226 UC-80-Reactor Technology.

Pilcher, J. M., R. I. Mitchell, and R. E. Thomas (1955) "The cascade impactor and particle-size analysis of aerosols," Proc. of 42nd Annual Meeting of Chemical Specialties Manufacturers Assoc. Inc., Dec. 6 & 7.

Ranz., W. E. and J. B. Wong (1952a) "Impaction of dust and smoke particles," I & E Chem., 44:1371.

Sonkin, L. S. (1946) "A modified cascade impactor," J. of Ind. Hyg. and Tox., 28:269.

Sparrow, E. M., S. H. Lin, and T. S. Longren (1964) "Flow development in the hydrodynamic entrance region of tubes and ducts," The Physics of Fluids, 7:338.

Stern, S. C., H. W. Zeller, and A. I. Schekman (1962) "Collection efficiency of jet impactors at reduced pressures," I & E C Fundamentals, 1:273.

Wells, B. J. (1967) "An evaluation of the May type of cascade impactor," Health Physics, 13:1001.

Wilcox, J. D. (1953) "Design of a new five-stage cascade impactor," A.M.A. Arch. Ind. Hyg. & Occup. Med., 7:376.

Zeller, H. (1965) "Large volume impactor collector," Applied Science Division, Litton Systems, Inc. 2295 Walnut Street, St. Paul, Minnesota 55113, Report No. 2893, Project No. 89125.

LIST OF FIGURES

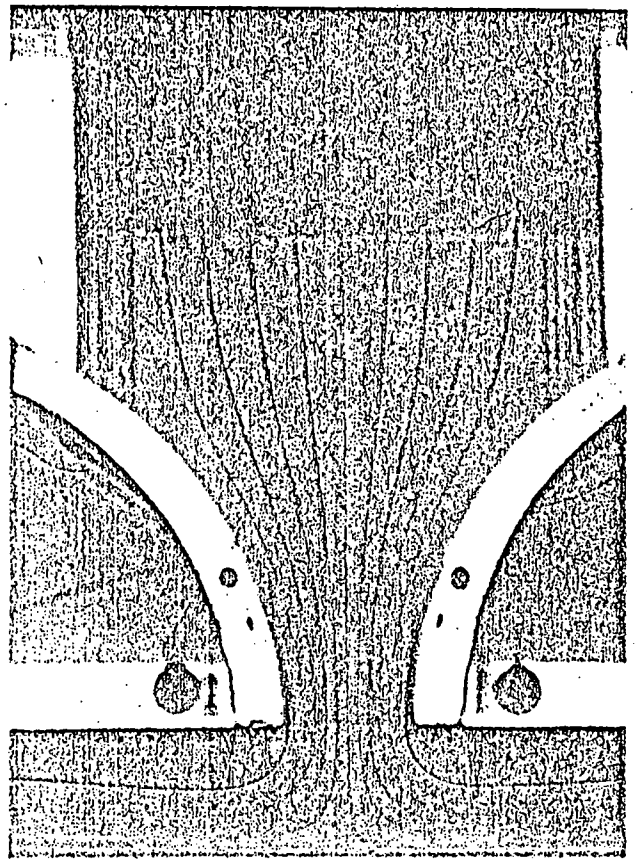

Figure 1 Experimental streamlines in the model rectangular impactor (Re = 700 and S/W = 1).

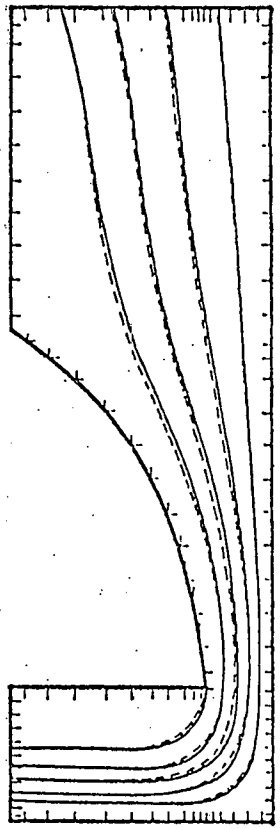

Figure 2 Comparison of the theoretical streamlines for two grid spacings (Re = 1000; —— grid spacings as shown along boundary, --- 1/2 grid spacing).

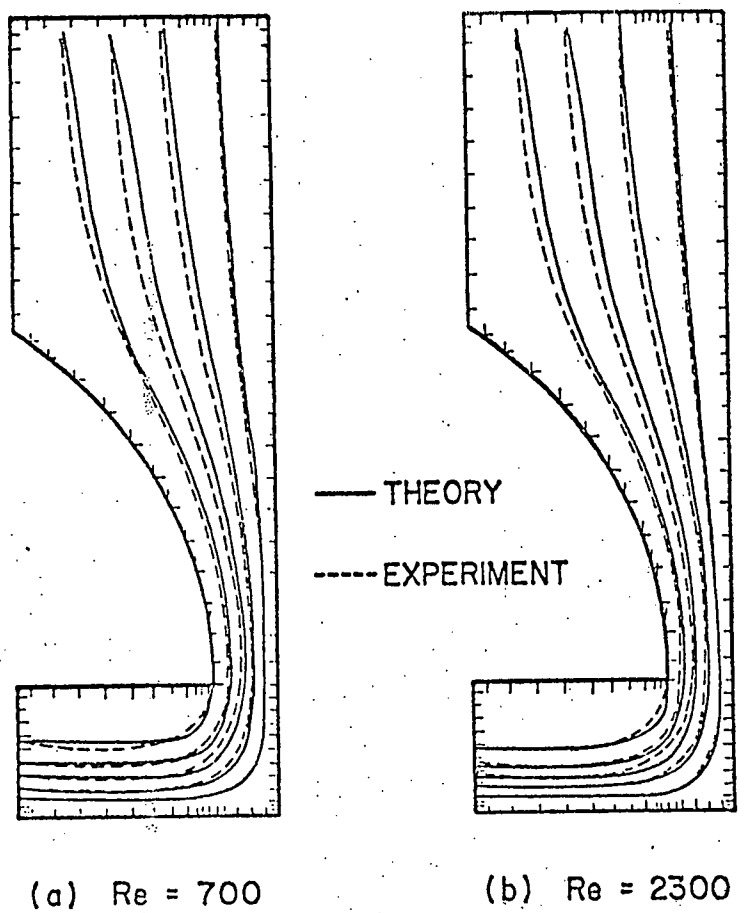

Figure 3 Theoretical and experimental streamlines for the rectangular impactor (S/W = 1).

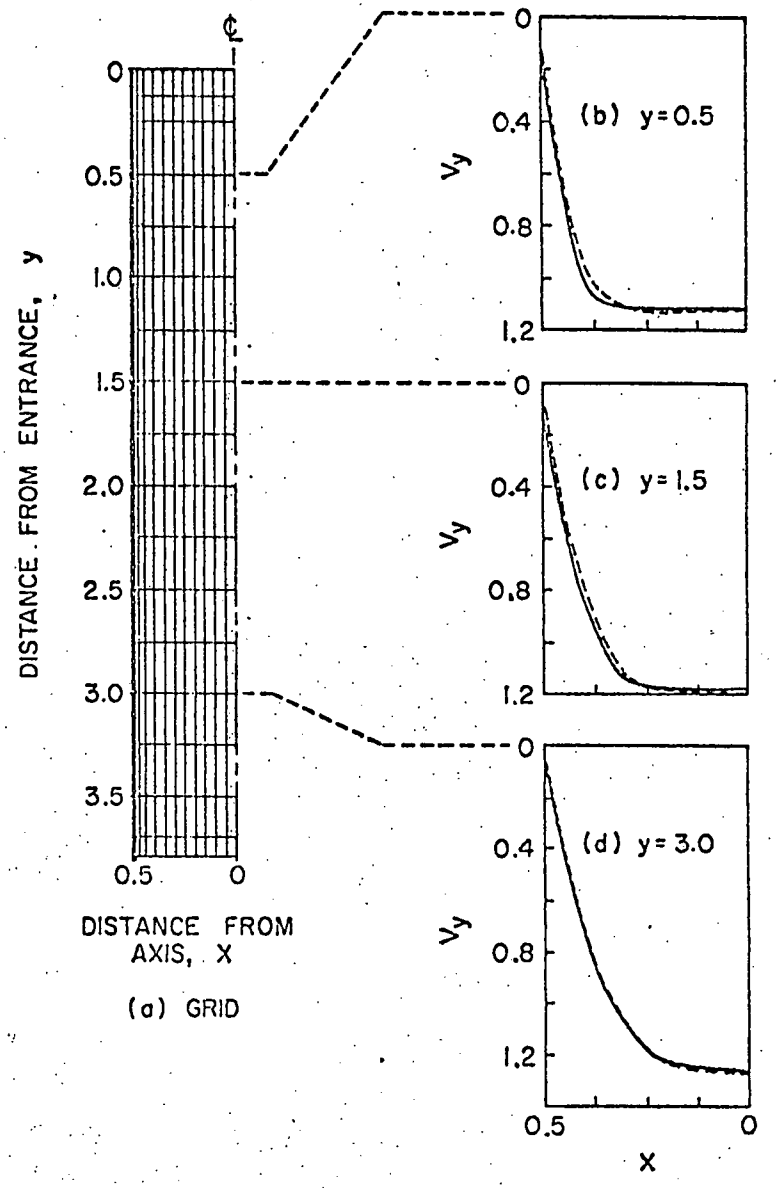

Figure 4 Grid pattern and velocity profiles in the entrance region of a parallel-plate channel (— analytical result of Sparrow et. al. (1964), --- present method).

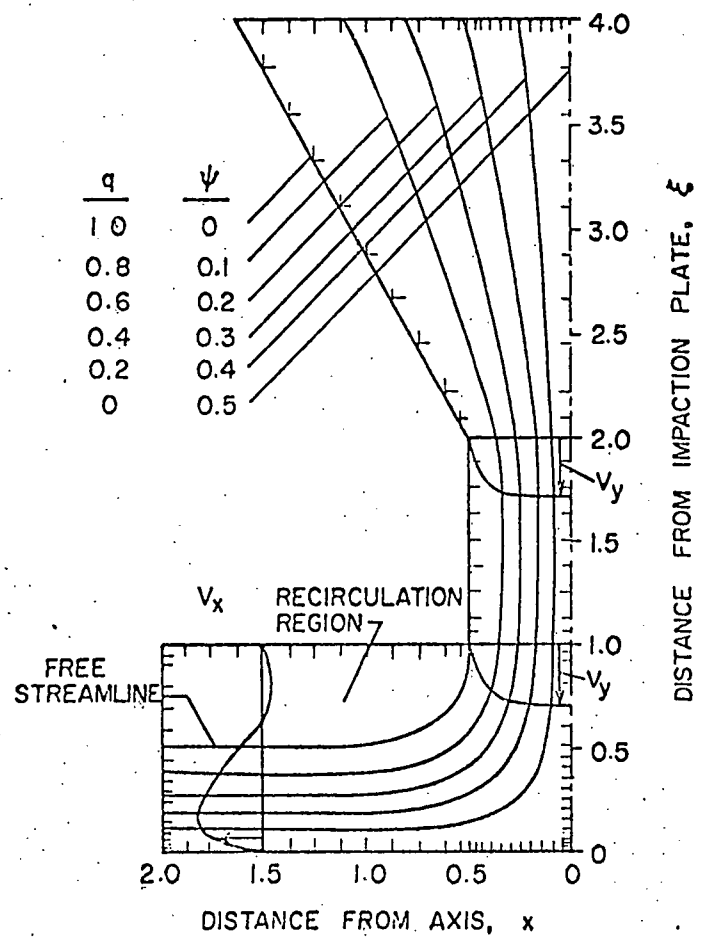

Figure 5 Theoretical streamlines and velocity profiles for the rectangular impactor (Re = 3000 and S/W = 1).

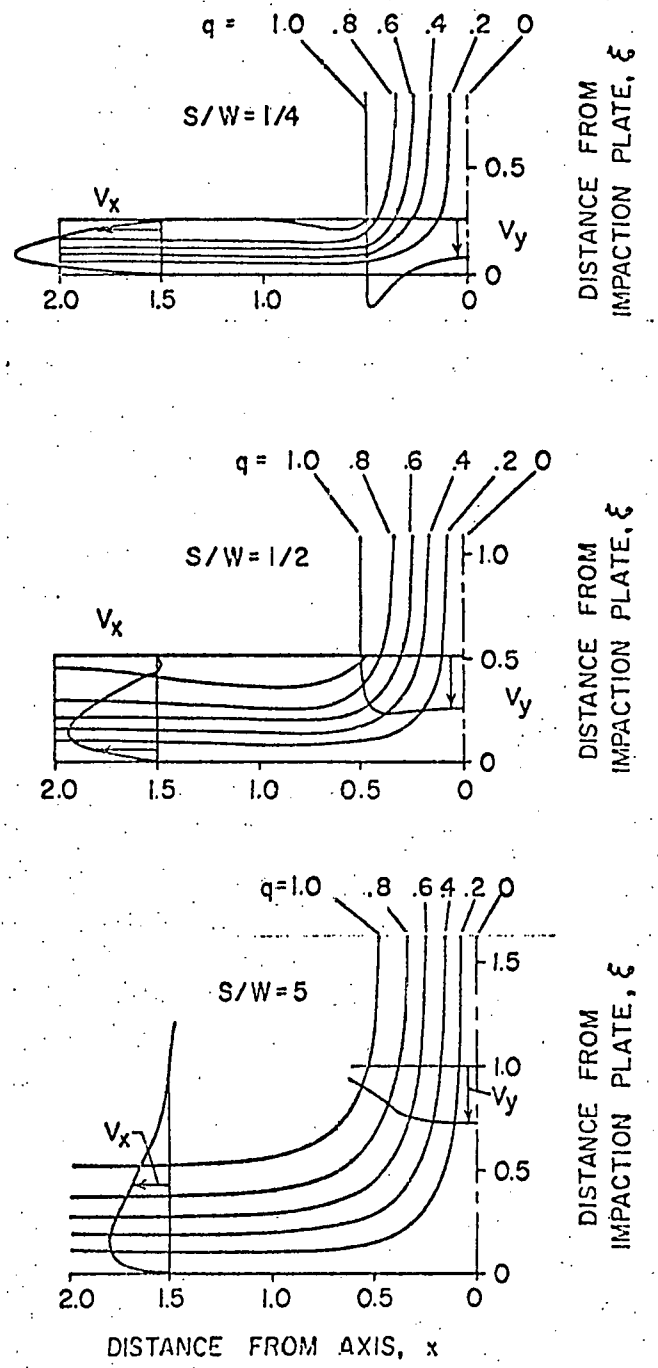

Figure 6 Theoretical streamlines and velocity profiles for the rectangular impactor (Re = 3000 and S/W = 0.25, 0.5, and 5).

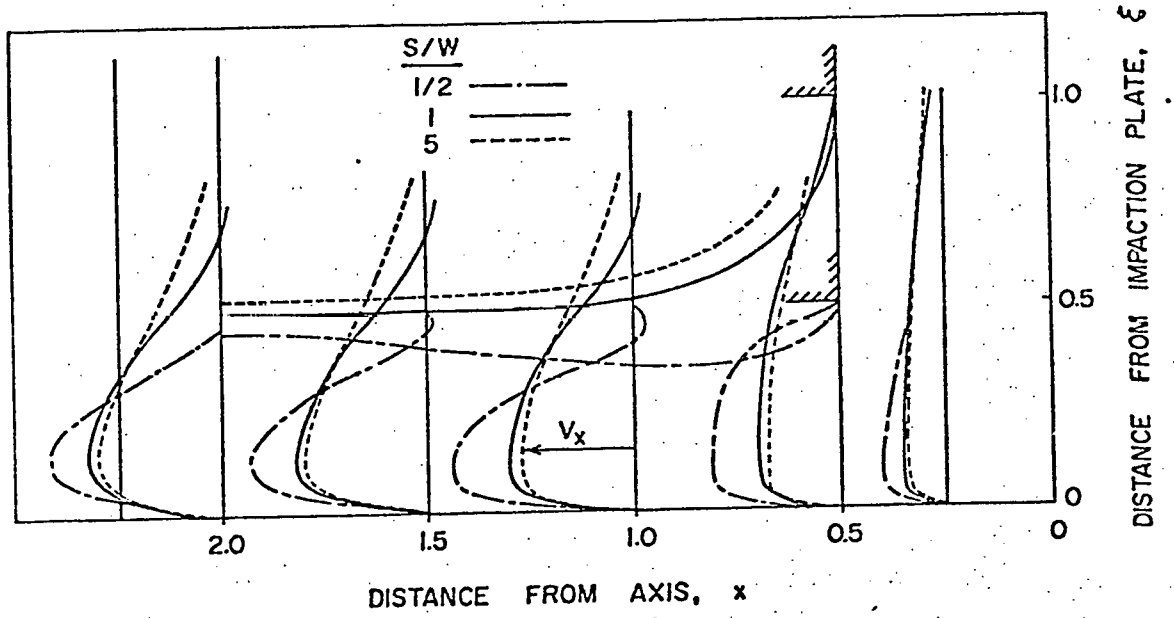

Figure 7 Theoretical velocity profiles, V_x along the impaction plate for the rectangular impactor (Re = 3000 and S/W = 0.5, 1, and 5).

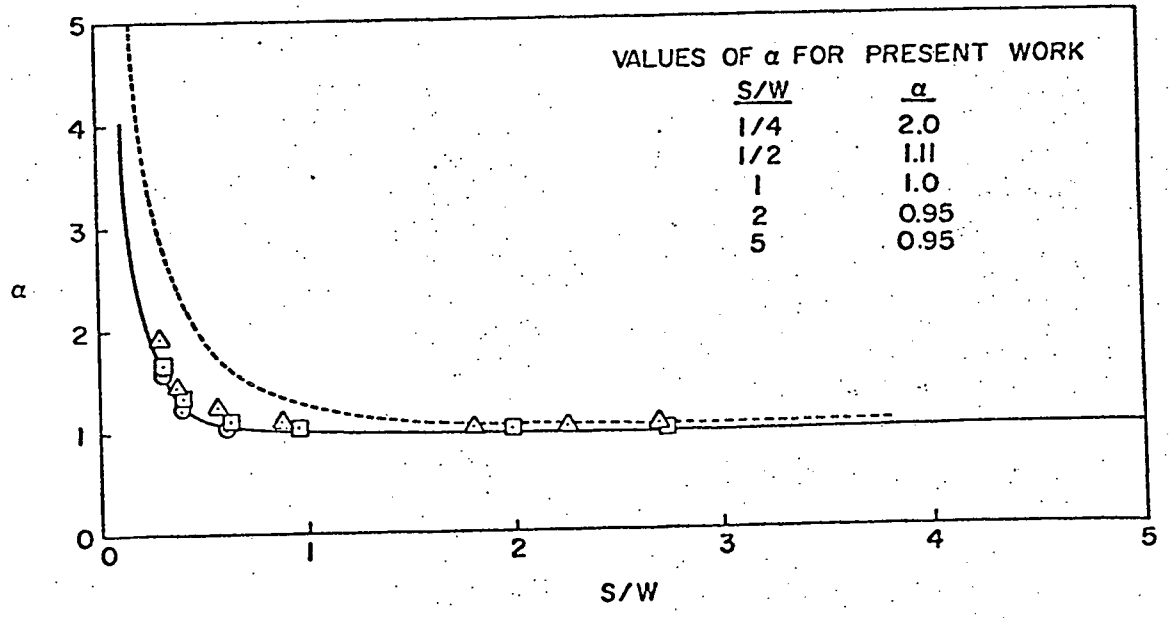

Figure 8 Variation of α with S/W for rectangular impactors (theoretical results; —— present work at Re = 3000, --- Davies & Aylward, 1951). (Experimental results; Mercer & Chow, 1968, at T/W = 0 (△), T/W = 1 (□) and T/W = 10 (○)).

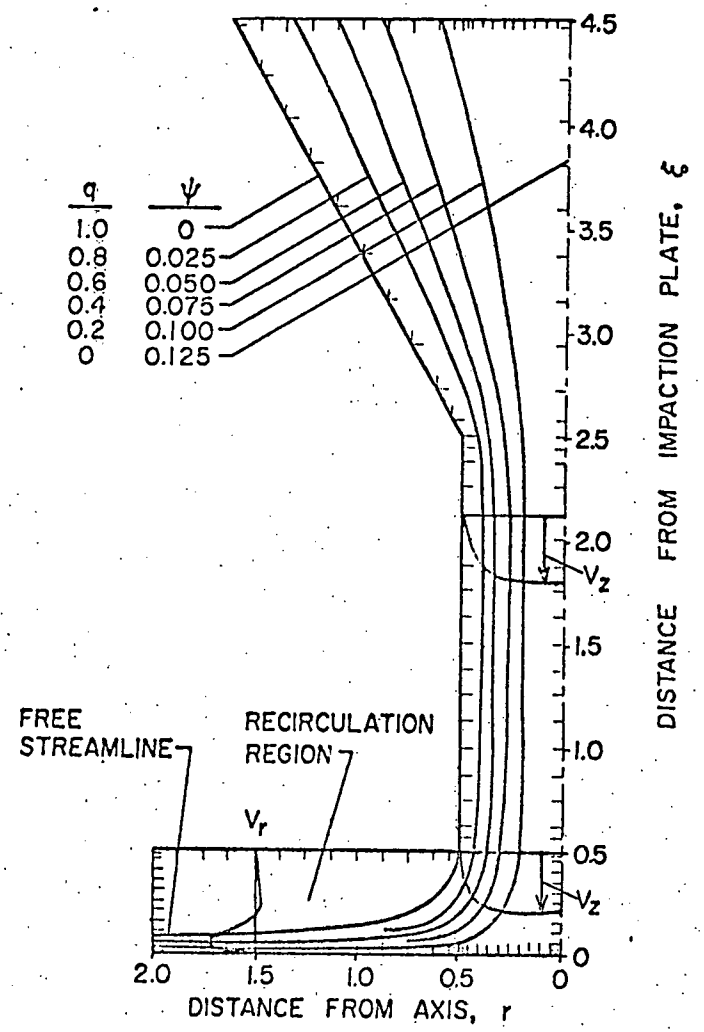

Figure 9 Theoretical streamlines and velocity profiles for the round impactor (Re = 3000, T/W = 2 and S/W = 0.5).

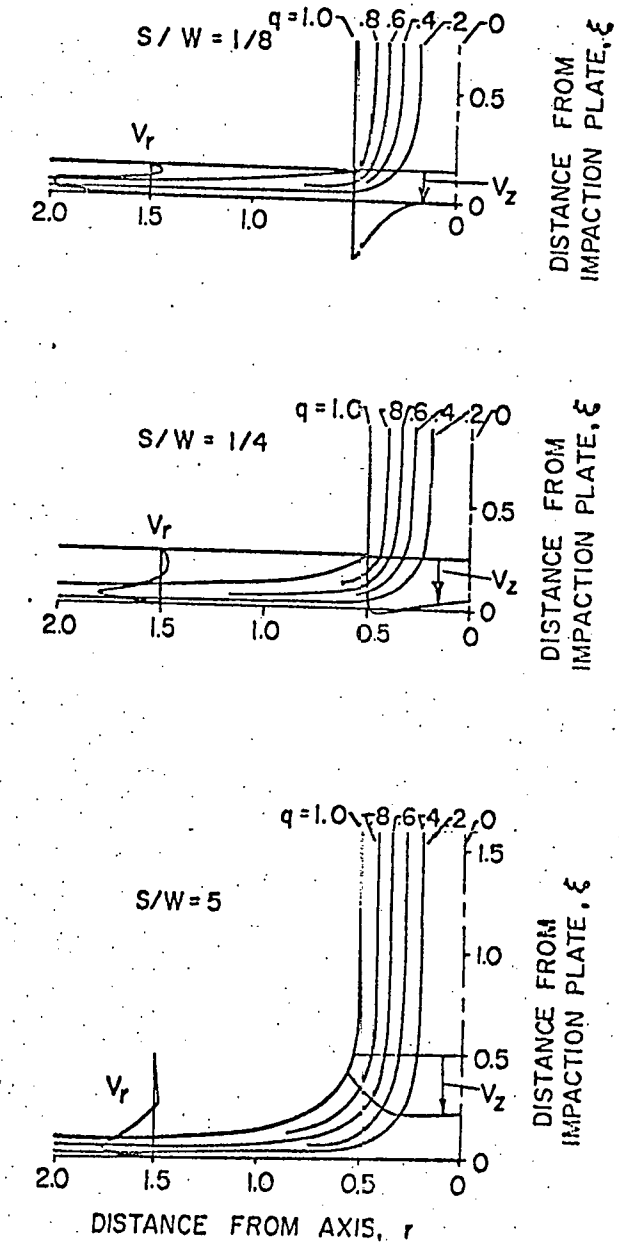

Figure 10 Theoretical streamlines and velocity profiles for the round impactor (Re = 3000, T/W = 2, and S/W = 0.125, 0.25 and 5).

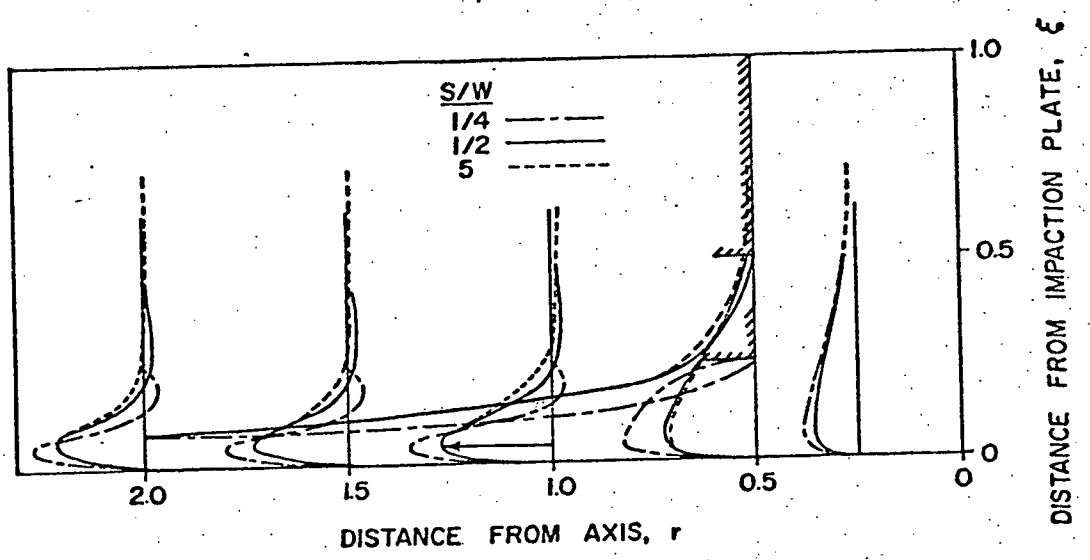

Figure 11 Theoretical velocity profiles, V_r, along the impaction plate for the round impactor (Re = 3000, T/W = 2 and S/W = 0.25, 0.5 and 5).

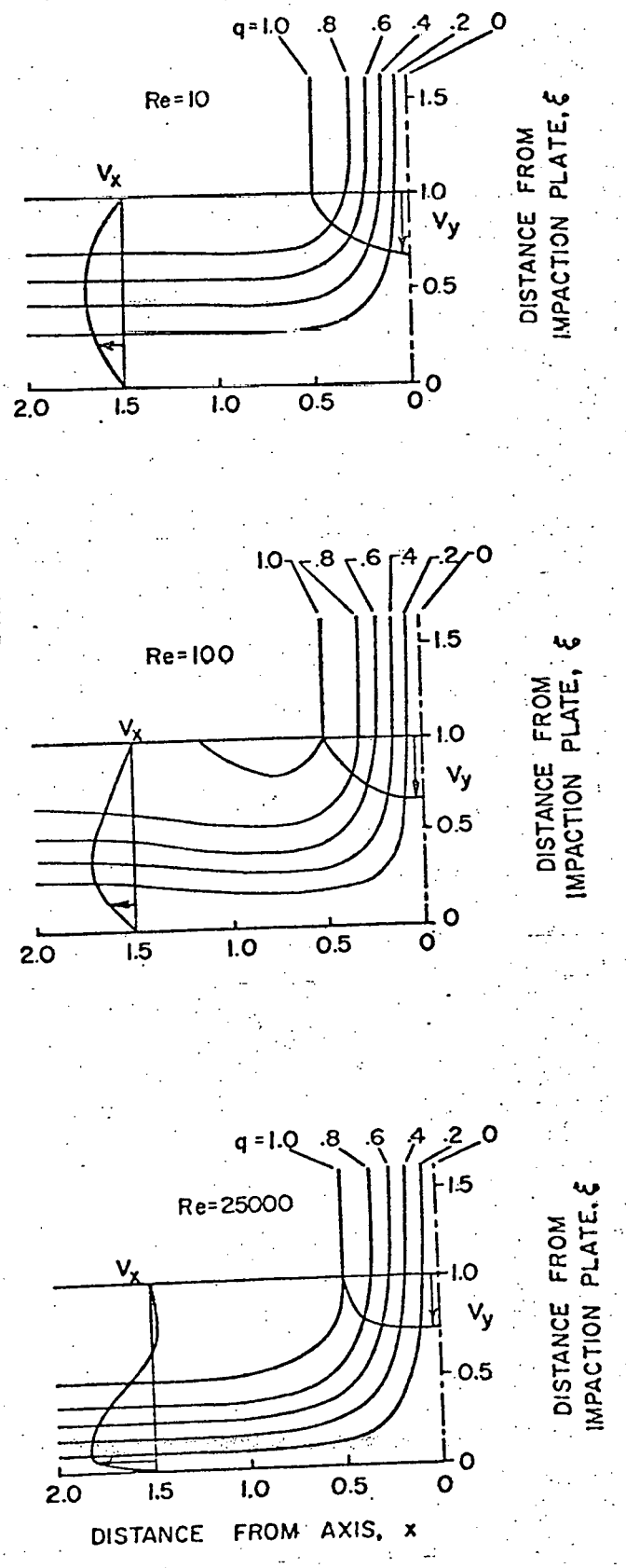

Figure 12 Theoretical streamlines and velocity profiles for the rectangular impactor (S/W = 1 and Re = 10, 100, and 25,000).

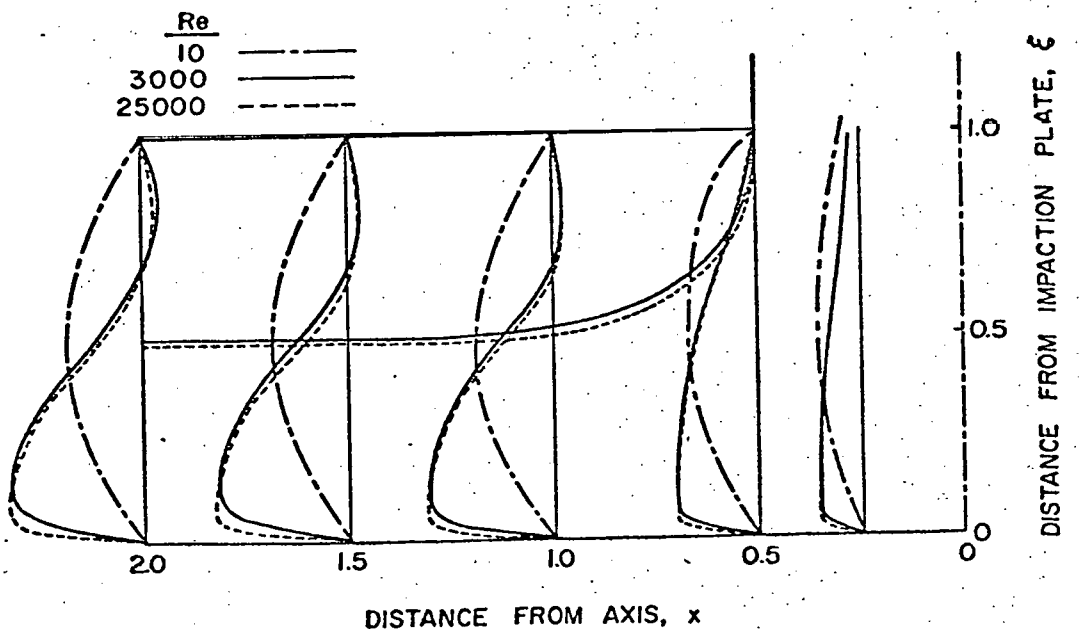

(a) RECTANGULAR IMPACTOR, S/W = 1

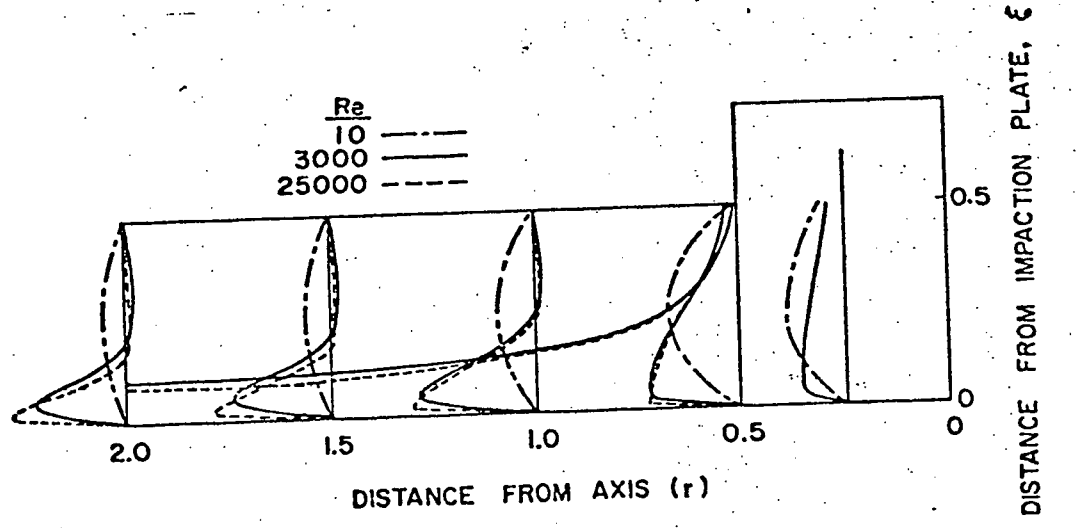

(b) ROUND IMPACTOR, S/W = 1/2

Figure 13 Theoretical velocity profiles along the impaction plate for the rectangular and the round impactor (Re = 10, 3000, and 25,000).

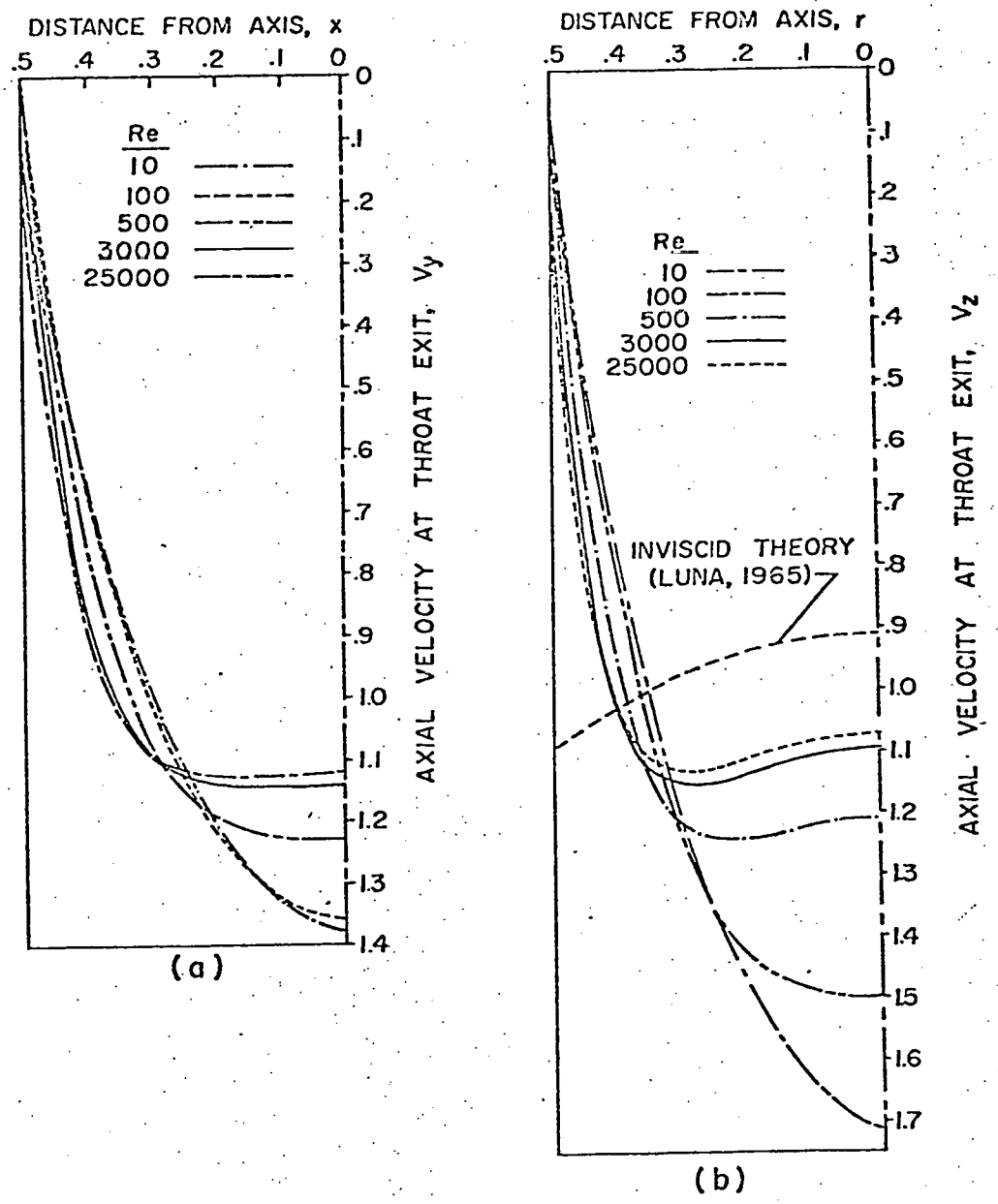

Figure 14 Axial velocity profiles at the throat exit for five Reynolds numbers (a) the rectangular impactor (S/W = 1) and (b) the round impactor (S/W = 0.5).